Dopant-induced Energetic Disorder in Conjugated
Polymers: Determinant Roles of Polymer-Dopant
Distance and Composite Electronic Structures

Michael Lu-Díaz^{1,‡}, Muhamed Duhandžić^{2,‡}, Simon Harrity¹, Subhayan Samanta¹, Zlatan Akšamija^{2,*}, and Dhandapani Venkataraman ^{1,3}*

(1) Department of Chemistry, 690 N. Pleasant Street, University of Massachusetts Amherst, Amherst, MA 01003; (2) Department of Materials Science and Engineering, University of Utah, 122 S. Central Campus Drive, Salt Lake City, Utah 84112-0056; (3) Materials Science and Engineering Interdisciplinary Graduate Program, University of Massachusetts Amherst, Amherst, MA 01003

KEYWORDS. Doped organic semiconductors, energetic disorder, densities of states, counterion distance, paracrystallinity.

ABSTRACT. Dopants induce energetic disorder in conjugated polymers and can adversely impact charge transport. In this work, we studied the dopant's impact on the density of states (DOS) of crystalline and amorphous domains in poly(3-hexylthiophene) (P3HT). We measured Seebeck coefficient-conductivity curves in films of doped regionegular and regionandom P3HT and their blends. These curves were simulated using a Gaussian disorder model. We also characterized the

undoped and doped films using X-ray scattering and near-infrared spectroscopy. Based on our studies, we conclude that the separation distance between the carriers on the polymer and the dopant anion is a crucial parameter that impacts dopant-induced disorder and depends on the morphology of the material. We also show that DOS distributions for both crystalline and amorphous regions are needed to understand charge transport over a broad range of doping levels. Our studies show that amorphous domains suffer a larger dopant-induced disorder but still contribute to charge transport. Thus, it is important to design dopants that minimize the dopant-induced disorder in both crystalline and amorphous domains.

Introduction

Conjugated polymers lack intrinsic free charge carriers and thus need to be oxidized or reduced to increase their conductivity. This simple process, termed chemical doping, introduces disorder by creating charge traps,¹ breaking percolation pathways,² and suppressing charge transport.³ As a result, it is challenging to predict doping levels needed for targeted charge transport properties.⁴ Dopant-induced disorder makes mobility highly dependent on doping through multifaceted polymer-dopant interactions.^{5, 6} Therefore, several recent studies have focused on identifying factors that affect polymer-dopant interactions and developing strategies to mitigate the dopant-induced disorder.⁷⁻⁹

Upon doping, conjugated polymers acquire a charge that is balanced by a counterion. The Coulomb interaction between the charge carrier and its counterion is poorly screened by the low dielectric medium of most polymers, which lowers the mobility of the carrier. Several studies have focused on identifying factors or properties that affect Coulomb interactions. 1, 10-14 A survey of the literature, however, shows that salient conclusions from these studies conflict. 8, 9, 15-20 Some studies correlate increased counterion size to reduced Coulomb interactions while others find no such

correlation and instead correlate increased molecular ordering^{18, 19, 21} with reduced Coulomb interactions. Moreover, translating molecular designs of undoped polymers with high mobility to doped polymers with high conductivity has been difficult. For example, indacenodithiophene-benzothiadiazole copolymer known for having an amorphous structure but with low energetic disorder²² showed field-effect mobilities significantly higher than many semicrystalline polymers,²³ but when doped, the conductivity of this amorphous polymer was low.¹⁸ As a result, consistent molecular design paradigms for high performance doped polymers have not emerged. Moreover, it is also common to model charge transport in conjugated polymers using the Gaussian Disorder Model based on a single density of states (DOS), with the implicit assumption that a single domain contributes to charge transport.²⁴⁻²⁶ Conjugated polymer films have both crystalline and amorphous domains; which domain dopants occupy and how each of these domains contribute to charge transport is not fully understood.²¹

In this study, we evaluate the impact of doping crystalline and amorphous regions on the DOS and therefore on the charge transport in doped conjugated polymer films. Poly(3-hexylthiophene) (P3HT) provides a powerful platform for such studies because the crystallinity of P3HT films depends on the polymer's regioregularity. We measured Seebeck coefficient and electrical conductivity in doped films regioregular P3HT, regiorandom P3HT and their blends. We analyzed the data using a phonon-assisted hopping model of charge transport that included the impact of dopant-induced disorder on the DOS. We characterized the doped films using wide-angle X-ray scattering and NIR spectroscopy. We show that each feature within the morphology of semicrystalline polymers concurrently contributes to charge transport, and their discrete contribution depends on the doping level. We also show that DOS distributions for both crystalline and amorphous regions are needed to understand charge transport over a range of doping levels.

We conclude that separation distance between the carriers on the polymer and the dopant anion is a reliable parameter that impacts dopant-induced disorder. We also posit that factors such as molecular ordering or counterion size impact the dopant-induced disorder if they alter the distance between the carriers on the polymer and the dopant anion. Our studies also show the importance of the impact of dopants in the amorphous domains of conjugated polymer films and the need for designing dopants that minimize dopant-induced energetic disorder in *both* crystalline and amorphous domains.

Experimental and Computational Methods

General Information: Regioregular P3HT (M_w : 26 kg/mol; Đ: 2.0; regioregularity: 96% Head-Tail) was purchased from Rieke Metals. Regiorandom P3HT (M_w ; 30-47 kg/mol; Đ=2.2-2.9; regioregularity: 1:1 (Head-Head:Head-Tail) was purchased from Sigma Aldrich. Iodine crystals were purchased from Sigma Aldrich. All solvents were purchased from commercial vendors.

Film Fabrication and Chemical Doping: 1.1 x 2.2 cm hand-cut glass slides were used as substrates for thermoelectric measurements and morphology studies, and quartz substrates were used for optical measurements. All substrates were sonicated with soap/water, water, acetone, and isopropanol for 10 min. each and dried in an oven at 130 °C. The substrates were cleaned under ozone (UVO Cleaner, Model 342, Jelight Company, Inc.) for 10 min.

Blends films of P3HT were prepared by dissolving appropriate proportions of regioregular P3HT and regiorandom P3HT (10 mg/mL) in chloroform and stirring overnight at 45 °C. The solutions were dropcast on preheated slides at 45 °C. Spincoated films were prepared by dynamic spincoating at 1,000 rpm for 1 minute followed by 2,000 rpm for 1 more minute. All films were

left under reduced pressure ($\sim 10^{-2}$ mbar) for at least 24 h to remove any residual solvents. The thickness of the films was measured with a profilometer.

The iodine doping-dedoping protocol consisted of exposing the films to iodine vapors and then to ambient conditions, as explained in our previous work. ^{10, 14} A 1 mL vial was loaded with 50 mg of iodine and placed inside a 20 mL vial. A polymer film was placed inside the 20 mL vial, adjacent to the dopant vial. The system was sealed under ambient conditions and heated in an oven at 75 °C for 2 h. Measurements were taken immediately after removing the film from the 20 mL vial. To ensure reproducibility, the measurements were done in triplicates for regionegular and regionandom polymers, and in duplicates for the blends (Figure S1).

Electrical Characterization: The film was placed in a glass slide between copper blocks with a temperature difference of about 18 °C. A custom-built four-point-probe apparatus with Pt probes was used. A Keithley 2400 sourcemeter was used to measure electrical conductivity. A Keithley 2182A Nanovoltmeter and a Matrix DT8852 thermometer with type K thermocouples were used to measure Seebeck coefficient.

Optical Characterization: Near-infrared spectra were obtained in a Varian 670 FT spectrometer. All measurements were performed in transmission mode on thin films deposited on quartz substrates.

X-ray Scattering: Wide-angle X-ray Scattering (WAXS) measurements were performed in a SAXSLAB Ganesha 300XL X-ray Scattering instrument equipped with a Xenocs GeniX 3D Cu $K\alpha$ source ($\lambda = 0.15418$ nm) and a Dectris Pilatus 30 K photon-counting detector. Free-standing films were prepared for transmission WAXS measurements.

Paracrystalline Disorder Parameter (g Parameter): The g parameter was calculated with the following approximation:

$$g = \frac{1}{2\pi} \sqrt{\Delta_q d_{hkl}}$$

where Δ_q is the Full Width at Half Maximum (FWHM) and d_{hkl} is the interplanar spacing of the peak of interest. This approximation does not account for lattice-parameter fluctuations.²⁷

Simulation of Seebeck coefficient vs electrical conductivity curves: We calculated Seebeck coefficient (α) and electrical conductivity (σ) based on a generalized Gaussian disorder model by numerically solving the Pauli master equation (PME) that describes phonon-assisted carrier hopping between localized sites whose energies are sampled from the carrier DOS. To capture the impact of dopant counter-ions on carrier states, we compute the DOS after doping by adding Coulomb interactions to GDM according to the modified Arkhipov model,²² which we have expanded with the ability to set the minimum spacing between dopant and polymer backbone as well as the spread of the charge on each dopant counterion. To accomplish this, we treated each dopant as a charge distribution having a Gaussian shape with standard deviation R_d rather than treating it as a point charge as it was done in the original model by Arkhipov et al.⁵ The maximum depth of the dopant trap is strongly influenced by the minimum spacing between dopant and carrier, which is determined by the location of the dopant counterions relative to the polymer backbone, here termed as polymer-dopant separation distance, R_s . Smaller R_s values lead to stronger interactions and produce a deeper tail in the DOS, representing deep traps, while a larger R_s limits the depth of traps and with it the heavy DOS tail. We noted this dependence in our earlier work.²⁸

Once the DOS of the doped polymer is computed, hopping of carriers between localized sites is determined from Miller-Abrahams rates. Further details of the implementation are given in our recent work.^{14, 28} Figure S1 shows the error associated with the simulated curves. To capture transport in films with multiple domains, we simulated an additional DOS in regionegular P3HT

with an offset of 0.1 eV between the DOSes that represent the amorphous and ordered regions. Energetic disorder caused by doping in each DOS is calculated separately according to their respective doping concentrations, before the final distributions were linearly added, which allows us to simulate the impact of doping in each region. In the simulation, we used a ratio of 1:1 for the number of states in ordered and disordered regions in regionegular P3HT, consistent with literature reports.²⁹

In general, the intrinsic energetic disorder, which is the width of the DOS before doping, can be obtained from experiments, e.g. Urbach tail measurements; however, such measurements capture the tail of the DOS and therefore only the ordered region nearest the bandgap. Studies that report the measurements of the whole DOS reveal a broader distribution of about 6 kT.³⁰ We set the disordered region, with a broader DOS of 7 kT, energetically below the center of the ordered region.^{31,32} The width of the DOS in the ordered region is 3 kT and the total width of the undoped regioregular system is about 6 kT. With the same method, we simulated blends of regioregular with regiorandom P3HT by keeping the DOS curves of the regioregular and regiorandom parts fixed to their values before blending, and then adding them in proportion to the blend ratio, as shown in Figure S2. The regiorandom DOS width is 3 kT and is centered at 0.25 eV below the center of the ordered regioregular region.³³

As noted earlier, dopant-carrier Coulomb interactions depend on polymer-dopant separation distance R_s . This R_s value represents the minimum distance between a charge and its nearest dopant. Separate values of R_s are assigned to each region according to its properties and used to compute the modified DOS of that region. Aligned side chains and π - π stacking in regionegular P3HT separate the dopant from the backbone, and we approximate the distance to be $R_s = 0.8$ nm. A report by Tashiro eta al. on iodine-doped P3HT places the dopant anion in a region at end of the

sidechain.³⁴ This data is also consistent with our WAXS data and the position of the (100) peak, which is a measure of the length of the side chains and width of the polymer backbone. From WAXS, d_{100} is 1.75 nm. Thus, placing the anion close to the end-methyl group of the sidechain would be slightly less than 0.875 nm ($d_{100}/2$). We note that R_s represents the effective minimum dopant-carrier distance from both regions in regioregular P3HT, crystalline and amorphous, since both are expected to have the same chain alignment and the crystalline domains differ from the amorphous in the overall alignment of the polymer chains rather than the orientation of the side chains. In the doped regiorandom P3HT, the side chain misalignment and the lack of π - π stacking allows the dopant to intercalate between side chains because of more free space in between. Therefore, we estimated R_s in regiorandom P3HT to be ~0.3 nm. This distance is consistent with the observed distance of 0.299 nm between counterion and the fused thiophene unit in the crystal structure of the dication—SbF₆ salt of 2,8-(tri-isopropylsilanyl)octathienoacene.³⁵

Calculation of Dedoping Rate: To calculate the dedoping rate in each domain of a polymer, we started from the diffusion coefficient $D = D_0 e^{-\frac{E_A}{kT}}$, where E_A is the activation energy. We connected this activation energy to the difference in energy between each carrier-occupied state on the host and the energy level of the dopant. This difference is the energy barrier for diffusion between the carrier and the dopant. To dedope, the electron on the dopant must return from the dopant (or other adventitious electron donor) energy level to some available state (which is represented by a hole) whose energy is higher by E_A . We take the dopant level to be aligned with the center of crystalline region of regioregular HOMO so that ΔE between them is zero. The regiorandom P3HT DOS is 0.25 eV below the regioregular crystalline region and the 0.25 eV difference in ΔE is considered in the regiorandom region. However, carrier energies are distributed around zero according to the DOS, which has a heavy tail at high doping concentrations, so that

carrier energies are above the dopant. This difference, E, is the activation energy for the transfer of an electron from the dopant back to the host polymer, that is, $E = E_A$.

Computationally, there is a distribution of E_A according to the DOS, so that the effective diffusion rate is:

$$D = D_0 \int dE \ e^{-\frac{E}{kT}} g(E) (1 - f(E)),$$

where we use g(E) for the doped DOS to avoid confusion with the diffusion coefficient, and f(E) is the Fermi function so that the term (1-f(E)) gives the probability that the state at energy E is unoccupied by an electron and can accept an electron from the dopant. If the surface concentration of dopants is zero (none in the air around the sample), then the concentration of dopants inside the sample, at a depth x, is simply given by:

$$C(x,t) = C_0 \operatorname{erf}\left(\frac{x}{2\sqrt{Dt}}\right),$$

where C_o is the initial (maximum) doping concentration at the start of dedoping. The average doping at time t is then:

$$C(t) = \frac{1}{L} \int_0^L C(x, t) dx = \frac{1}{L} C_0 \int_0^L \operatorname{erf}\left(\frac{x}{2\sqrt{Dt}}\right) dx,$$

where L is the sample thickness. For $\sqrt{Dt} \ll L$, the solution is $C(t) = \frac{1}{L}C_0\left(1 - \frac{2}{\sqrt{\pi}}\frac{\sqrt{Dt}}{L}\right)$. In the opposite limit, the expression becomes $C(t) = \frac{1}{L}C_0\left(\text{erf}\frac{L}{2\sqrt{Dt}} + \frac{2\sqrt{Dt}}{\sqrt{\pi}L}\left(e^{-\frac{L^2}{4Dt}} - 1\right)\right)$.

We calculated D readily from our simulations for each carrier concentration n, but the time dependence of D cannot be computed directly as it requires tracking the concentration of dopants over time. We started from D at the maximum doping (in our case 50%) and calculate the doping concentration after a very small timestep. We then calculated D at that doping concentration by

interpolation and used the new D in the next timestep. Repeating this procedure for every point, we obtained the plot of C(t) vs. t. We used this information to obtain $\sigma(t)$ by interpolation $\sigma(n)$. Doping, and with it the dopant diffusion rate and conductivity, depend on time and sample depth, but decay in the limit $\sqrt{Dt} \ll L$ as $1 - \frac{\sqrt{Dt}}{L}$. However, this decay is not exponential as opposed to what we see in experiments. This is because the rate D is a function of doping concentration.

Absorption Spectra: To fit our experimental data from regioregular P3HT samples, we simulated the α vs. σ curve starting with a DOS containing two contributions, one for amorphous domains and another one for crystalline domains. Next, we utilized that same two-component DOS to simulate the absorption spectra. We calculated the absorption rate from the sum of all transition rates as:

$$r_{abs}(\omega) = \sum_{i,j} W_{ij} f(E_i) \left(1 - f(E_j) \right) \delta(E_i - E_j + \hbar \omega_{ph}),$$

where f is the Fermi-Dirac distribution function of carriers, $\hbar \omega$ is the energy of incident photons, and W_{ij} is the transition rate between sites (i-j).³⁶ Subtracting the spontaneous emission, which is proportional to $(1 - f(E_i))f(E_j)$, and grouping out the constants gives the absorption coefficient as:

$$\alpha_{ph}(\omega) \propto \frac{A}{\omega} \sum_{i,j} \left(f(E_i) - f(E_j) \right) \delta(E_i - E_j + \hbar \omega),$$

where A is a constant, which we omitted for further consideration as our absorption rates will be normalized. When the material is not crystalline and momentum is not conserved in optical transitions, it is possible to split the delta function into a product $\delta(E_i - E_j + \hbar\omega) = \delta(E - E_i) \cdot \delta(E - E_j + \hbar\omega)$, which then gives the convolution:

$$\int dE \ g(E)g(E+\hbar\omega).$$

Absorption coefficient is then proportional to:

$$\alpha_{ph}(\omega) \propto \frac{1}{\omega} \int dE \left(f(E) - f(E + \hbar \omega) \right) g(E) g(E + \hbar \omega)$$

After we computed the doped DOS and Fermi function, we obtained the absorption coefficient numerically. We interpolated $g(E + \hbar \omega)$ for each frequency of incident light and integrate over the whole energy space. Lastly, we converted the angular frequency ω of the photons to wavelength and normalized the absorption coefficient for each case of polymer and blend.

Results and Discussion

We prepared thin films using different compositions of regionegular and regionandom poly(3-hexylthiophene). Figure 1a (top) shows the ratios of polymer blends used in this study. Throughout this manuscript, we denote the composition of the blend as the ratio of each component and not as the total regionegularity of the component. For example, 100% regionegular P3HT represents a sample with regionegular P3HT (96% regionegularity) only whereas a 50% regionegular P3HT sample is composed of 1:1 blend of regionegular and regionandom P3HT. We doped these polymers by exposing the films to iodine vapors in a sealed chamber and then measured the Seebeck coefficient (α) and electrical conductivity (σ) simultaneously as the films dedoped, as previously published.^{10, 14}

In Figure 1, we show α—σ curves for regiorandom P3HT, regioregular P3HT and their blends. At the highest level of doping, 100% regioregular P3HT film showed the highest conductivity whereas 100% regiorandom P3HT showed the lowest conductivity. The conductivity of the blends is in-between and increases with increased fraction of regioregular P3HT. Previously published literature for F₄TCNQ doped samples shows that the highest conductivity for P3HT is achieved at different regioregularity content, ranging from 50% up to 90% regioregularity.^{21, 37} Interestingly,

the α - σ plot shows a slightly different picture in that the order of the curves does not follow the progression of the blend composition.

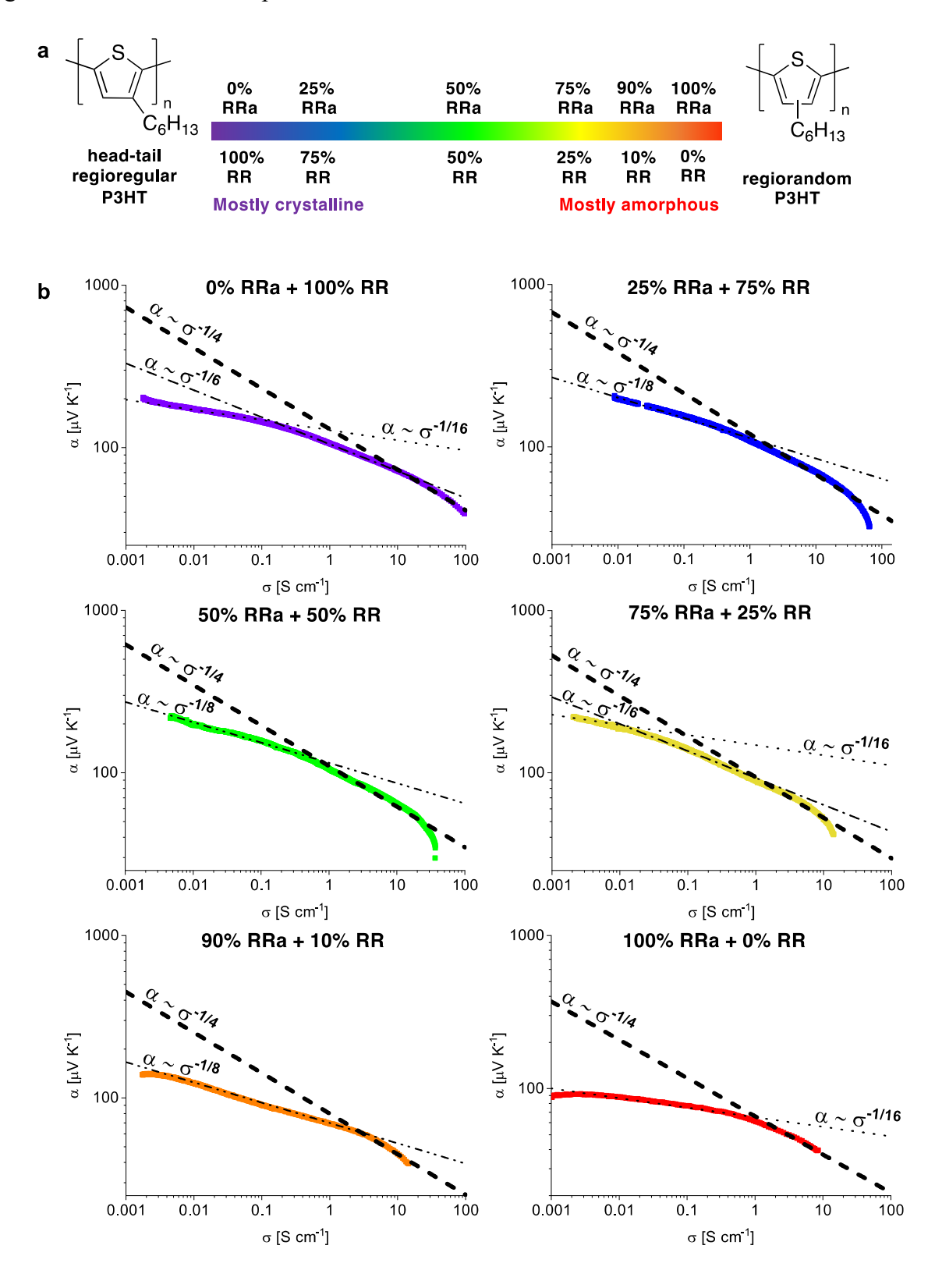


Figure 1: Impact of regioregularity on thermoelectric properties of polymer films. (a) Chemical structures for regioregular (RR) and regionandom (RRa) P3HT. Blends prepared with a different composition of regionandom to regionegular P3HT. (b) Power law fits to Seebeck-electrical conductivity curves of regionegular-regionandom blends indicate a non-universal power law dependence.

It has become common in the literature to fit α - σ data to an empirical power law ($\alpha \sim \sigma^{1/4}$), $^{2, 38-42}$ even though the universality or the physical origin for this relationship is yet to be established. $^{15, 43-45}$ When we fit out data to this power law, we found that only a narrow set of data, at the high doping regime, fit to this power law (Figure 1b). We also found that different sections of the curve fits require different exponents ranging from -1/16 to -1/4. We analyzed the data from the blends and found that this often-used power law with -1/4 exponent does not capture the α - σ data over a broad range of doping concentrations. The slope of the Seebeck coefficient-conductivity curve changes as the function of the dopant concentration, which confirms that the electronic structure changes as the sample dedopes, which has been noted before 15 but the full connection between doping, electronic structure, and transport has not been elucidated.

To understand the trend in the curves, we first examined the role of doping on paracrystallinity using Wide-angle X-ray Scattering (WAXS) in transmission mode (Figure 2). Figure 2a shows the scattering pattern of all undoped blends. We fitted the scattering pattern to multiple Gaussian distributions to resolve each peak (Figure S3). For undoped regioregular P3HT, the main peaks for (100) and (010) appear at 0.38 Å⁻¹ and 1.67 Å⁻¹, respectively, and represent lamellar stacking and π - π stacking.²¹ The (100) appears as a sharp peak amidst a broad peak. The (010) also appears as a sharp peak amidst a convolution of broad peaks between 0.9-2.1 Å⁻¹. We attribute these broad peaks to the amorphous portion of this polymer. Undoped regiorandom P3HT also shows (100)

and (010) peaks, but they are broad. The (100) has a shoulder at slightly higher q values, which fits to another broad Gaussian distribution with smaller intensity than the main peak (Figure S4). Unlike regionegular P3HT, the (010) peak fits to a single Gaussian distribution and has no sharp peak in this region. Yee, et. al. previously reported the existence of broad scattering peaks in undoped regionandom P3HT, which is associated with the structural disorder of this polymer.⁴⁶

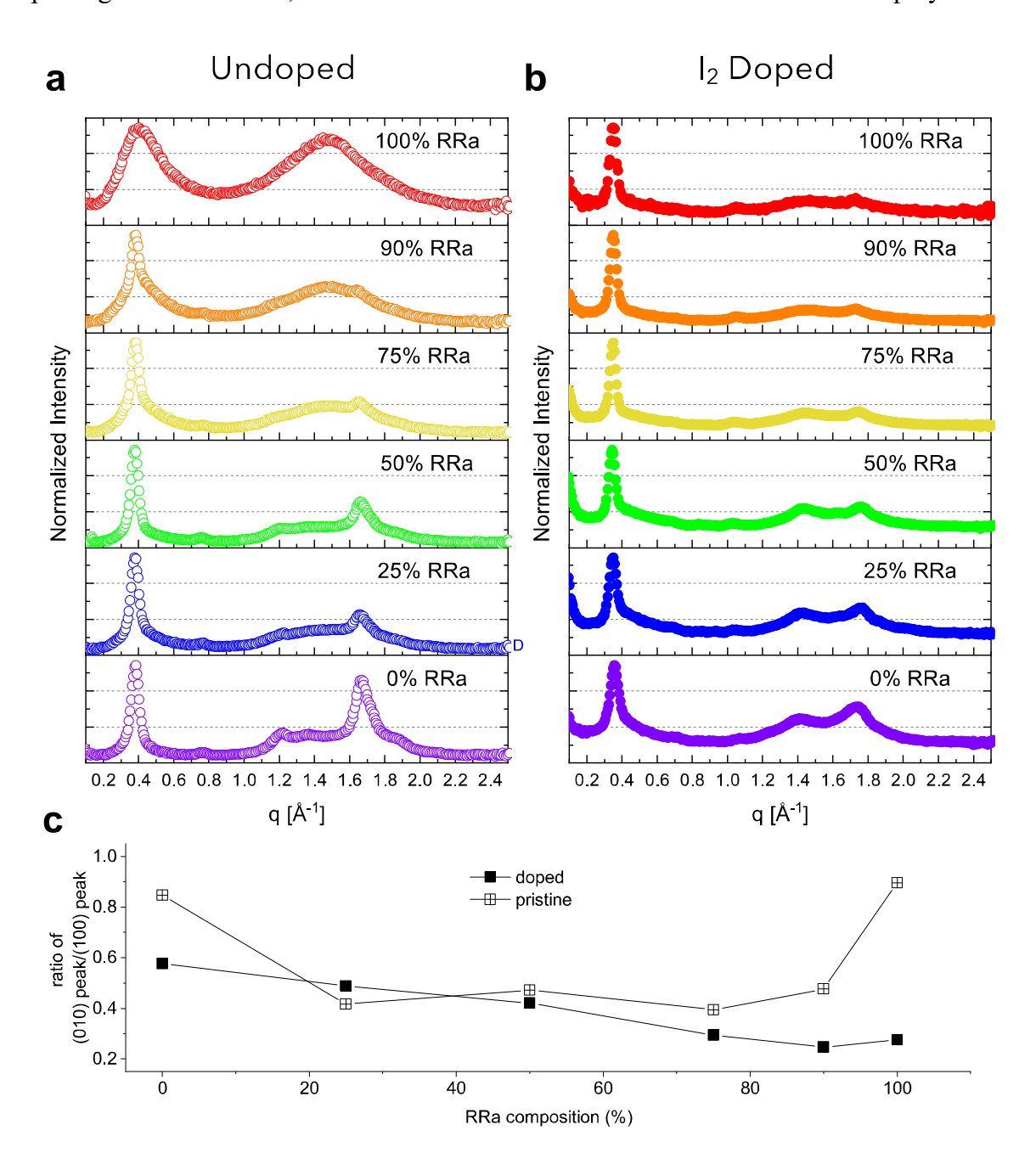


Figure 2: Wide-Angle X-ray Scattering of undoped and Iodine doped P3HT. X-ray Scattering pattern of (a) undoped P3HT and (b) Iodine doped P3HT. (c) Intensity ratio for π - π stacking peak to lamellar stacking peak shows a reduction with increasing regionandom P3HT content. This ratio was calculated based on the intensity of Gaussian distribution fits of the peaks with the highest intensity for both types of polymer packing.

Upon doping, the (100) peak shifts to a lower q value whereas the main (010) peak shifts to a higher q value (Table S1). We found an increase in lamellar spacing from ~ 16.5 Å to ~ 17.5 Å, and a decrease in π - π stacking distance, from ~3.76 Å to ~3.62 Å. Previous literature shows this expansion and contraction of the polymer lattice in the presence of dopants.^{31, 32} Another peak that represents the π - π stacking emerged at lower q values (~1.41 Å⁻¹) and is labeled as (010)*. This peak has been previously associated with amorphous domains.⁴⁷ We observed that the q values for the (100) and (010) peaks are similar between the blends, indicating that the polymer morphology is similar in all the doped blends. The (100) peak for doped regiorandom P3HT becomes significantly narrower after doping. To quantify structural disorder and analyze changed upon doping, we calculated a paracrystallinity disorder parameter (g parameter) for (100) and (010) peaks, as described in the Methods section. The g parameter provides a metric for the overall structural disorder in the structure associated with a particular peak. 18, 27, 48 In undoped samples, we observed that (100) peak had a higher g value ($g \sim 14\%$ for regionegular P3HT and $\sim 30\%$ for regiorandom P3HT) compared to (010) peak ($g \sim 9\%$ for regionegular P3HT and $\sim 26\%$ for regiorandom P3HT). The g-parameter increases as the fraction of regiorandom P3HT increases, indicating an increase in structural disorder. Using Raman and photoluminescence spectra, Salleo and co-workers showed that doping regionandom P3HT with F4TCNQ leads to increase in conjugation length.³⁷ Previous literature on regiorandom P3HT doped with F₄TCNQ shows strong scattering peaks in GIWAXS associated with lamellar and π - π stacking and concluded that dopants induce structural order in regionandom P3HT.^{21, 46} Thus our observations in iodine-doped regionandom P3HT are consistent with observations in F₄TCNQ doped regionandom P3HT.

Upon doping, the g-parameters for the peaks do not change significantly with an increase in regiorandom P3HT fraction. All blends show g parameters in the range of 14-16% for (100), 15-16% for (010), and 17-19% for (010)*, which indicates that the paracrystallinity is similar regardless of the regioregular-regiorandom composition. The only exception was 90% RRa and 100% RRa, which had low intensity (010) peaks that were hard to resolve, thus the g parameter was not reported. We observed that the intensity ratio of the (100) peak to the (010) peak decreases with increasing regiorandom P3HT fraction in the blend. In undoped samples, the ratio decreases with the addition of 25% regiorandom, stays roughly the same for the blends and increases again for regiorandom P3HT (Figure 2c). The steady decrease in the $I_{(001)}/I_{(010)}$ in doped samples of the blends indicates that while doping can increase the conjugation length in regions that resemble regiorandom P3HT due to increased co-planarity of the thiophene rings and increased order along (100), the dopant may be disrupting or suppressing the π - π stacking. This implies that (1) dopants can get very close to the polymer backbone in samples with higher regiorandom content, and that (2) dopants can penetrate different regions depending on the regioregular/regiorandom content.

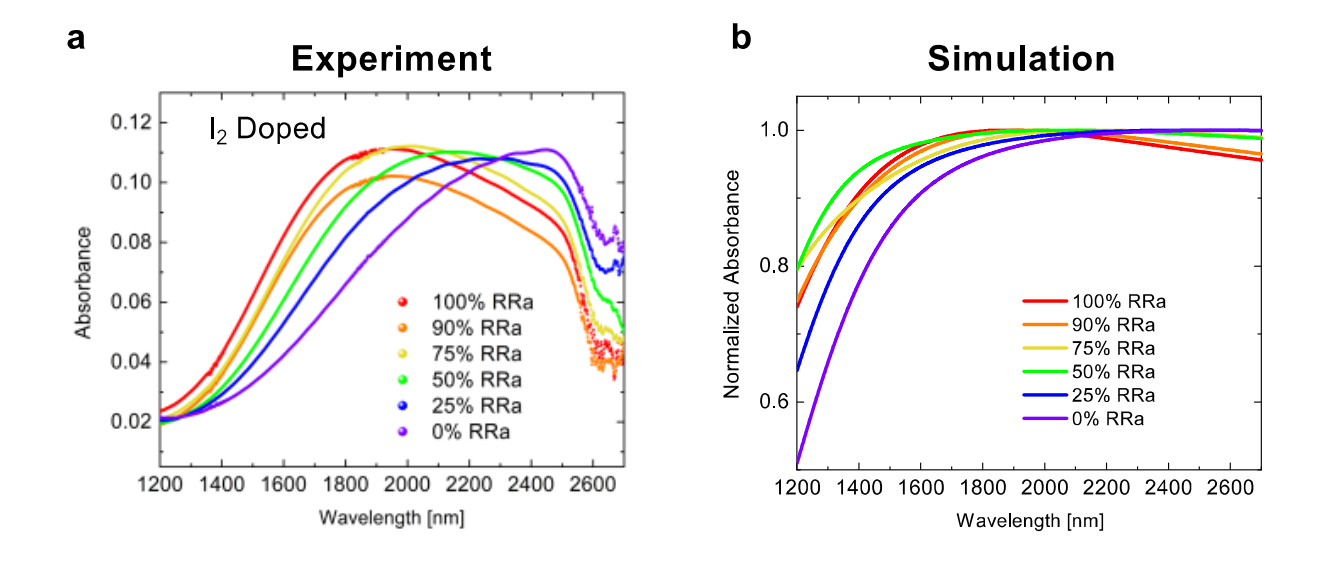


Figure 3: Probing polymer-dopant distance through NIR. (a) Experimental NIR spectra of doped P3HT blends shows a red shift for iodine doped regionegular P3HT with regards to iodine doped regionandom P3HT. (b) Simulated NIR spectra also shows a redshift for doped regionegular P3HT and blends with highest content of the same.

We then used Near Infrared Spectroscopy (NIR) to study the polaron peaks in doped samples. Schwartz, et. al. used this tool together with a theoretical model to conclude that a NIR peak shift in P3HT arises from a combination of delocalization induced through increased crystallinity and through tuning the polaron-counterion distance. ⁴⁹ Our data (Figure 3a) shows that the polaron peak for samples with high regiorandom P3HT content appears at shorter wavelengths compared to samples with high regioregular P3HT content. From our g parameter analysis, we concluded that the paracrystallinity of highly doped blends is similar, therefore crystallinity-induced effects of the location of the peak should be minimal. We believe that the peak shift is associated with the extent of delocalization of the polaron, which in turn is correlated to the polaron-counterion distance ⁵⁰ — a blue shift may indicate a smaller R_s whereas a red shift may

P3HT is calculated with an R_s =0.8 while that of regiorandom P3HT with an R_s =0.3 nm, as detailed in Methods and further discussed in the context of transport. The DOSes of the blends were obtained by combining the two according to their respective fractions in the blend. Thus, a 50% regiorandom P3HT blend contains the DOS of the regiorandom P3HT multiplied by a half plus the regioregular DOS, which is itself already a combination of crystalline and amorphous contributions to its DOS, also scaled by a half. Spectra calculated from transitions between states in the resulting combined doped DOS qualitatively agree with the experimentally observed trends (Figure 3b), confirming that the shift is caused by the heavier tail in the DOS. This tail is produced by stronger Coulomb interactions in regiorandom P3HT when dopant counterions are closer to the polarons. States deeper in the heavy tail allow for larger photon energies to be absorbed, resulting in the blue shift relative to regioregular P3HT, which has a smaller R_s and a lighter DOS tail.

Most studies examine charge transport in conjugated polymer films as arising from the crystalline domains only and thus model charge transport using a single density of states, while amorphous domains are expected to have deep trap states and thus are often assumed not to contribute to charge transport.⁵¹ From our conductivity data, we can evaluate the kinetics of dedoping (Figure 4a). If only a single component contributes to the conductivity, then we should be able to fit the rate with a single first order process. For regionandom P3HT, this is indeed the case as the rate of change in conductivity can be fit to a single first order process (Figure 4b) with a rate coefficient of 0.03 min⁻¹ (Table S2). All other samples require at least two concurrent first order processes to fit the data, including doped regioregular P3HT (see Figure 4c). We found that the fast process of regioregular P3HT has a rate coefficient similar to the first order process used to fit regiorandom P3HT. The slow process has a rate coefficient that only fits to part of the

dedoping rate of regioregular P3HT. In essence, the kinetic data for regioregular P3HT has both a slow process and a fast process while the kinetic data for regiorandom P3HT only has a fast process. Based on the similarities of rate coefficients and the absence of a slow process in regiorandom P3HT, we associate the fast process with amorphous domains and the slow process with crystalline domains. Thus, at high doping both crystalline and amorphous domains contribute to charge transport. As amorphous domains de-dope faster, the crystalline domains become dominant at low doping regions, and this is reflected in the Seebeck-conductivity curve.

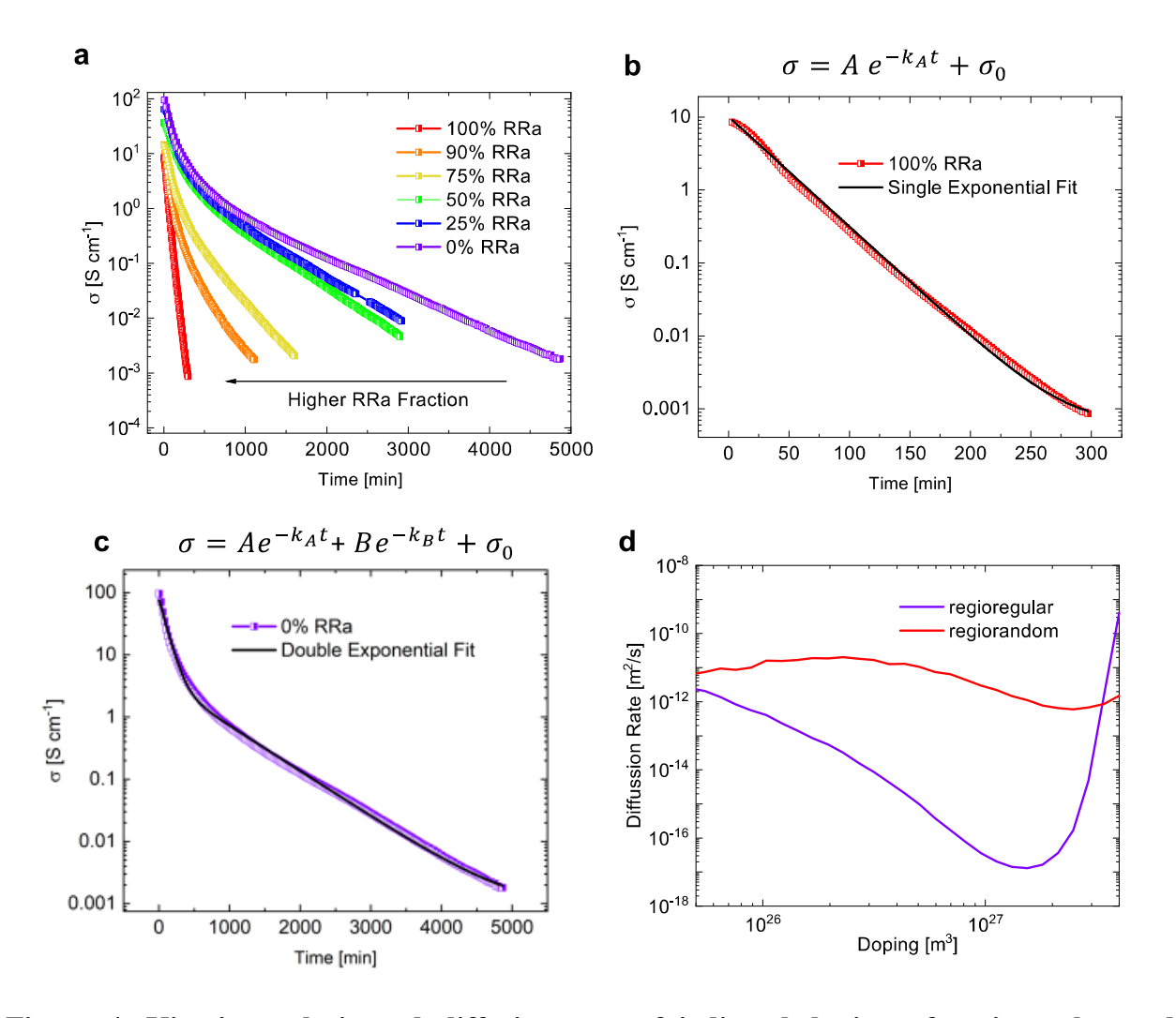


Figure 4. Kinetic analysis and diffusion rate of iodine dedoping of regioregular and regiorandom P3HT show a contribution from multiple structural entities. (a) Electrical

conductivity of polymer blends with different regioregular (RR) to regiorandom (RRa) content as a function of time. (b) Regiorandom P3HT fits to a single exponential decay rate, indicating dedoping of one type of domain. (c) Regioregular P3HT fits to two exponentials, indicating dedoping of two types of domains. (d) Diffusion coefficient of regioregular and regiorandom P3HT show that regiorandom P3HT has a faster diffusion rate within this doping level range.

From a molecular chemistry perspective, because the HOMO of regionegular P3HT (~-4.6 eV) is higher than regiorandom P3HT (~-4.9 eV),33 we can reason that the holes are more stable on regioregular P3HT compared to regiorandom P3HT. Thus, we would expect that regioregular P3HT to dedope slower. We also considered the possibility that the counterions can get closer to the polaron in regiorandom P3HT and thus can stabilize the polaron via strong Coulomb interactions. However, this possibility is not supported by our experimental data as we observed that regiorandom P3HT dedopes faster and WAXS data of doped regiorandom P3HT shows that the π - π stacking is disrupted indicating that the counterion can get closer to the polaron. NIR data is also consistent with a smaller R_s . To understand which parameter controls the dedoping kinetics of doped P3HT, we simulated dedoping rates using the same procedure to obtain the doped DOS of regioregular and regiorandom P3HT as for the NIR spectra. We then computed the dedoping rate from the dopant activation energy, which is the energy difference between the dopant level and each available state in the DOS (more details in Methods section). The computed diffusion coefficients in Figure 4d show that regionandom dedopes faster at nearly all doping concentrations despite having a heavier DOS tail, in agreement with the experimental kinetic data. In both regioregular and regiorandom P3HT, when the sample is highly doped, the Fermi level is closer to the middle of the DOS where the dopant level is located, which makes electron transfer from the dopant to the hole state easy to be thermally accessible. At low doping levels, only states in the

tail have holes that can accept the electron from the dopant so dedoping requires large energy, making dedoping slower. This effect is more pronounced in regiorandom P3HT due to the larger offset of the dopant level, resulting in faster dedoping. Although our simulations indicate that the R_s can also impact the diffusion rate (Figure S5), the main parameter that controls dedoping in P3HT is the energy offset between the polymer and the dopant, and it is reflected in our simulated data (Figure 4d).

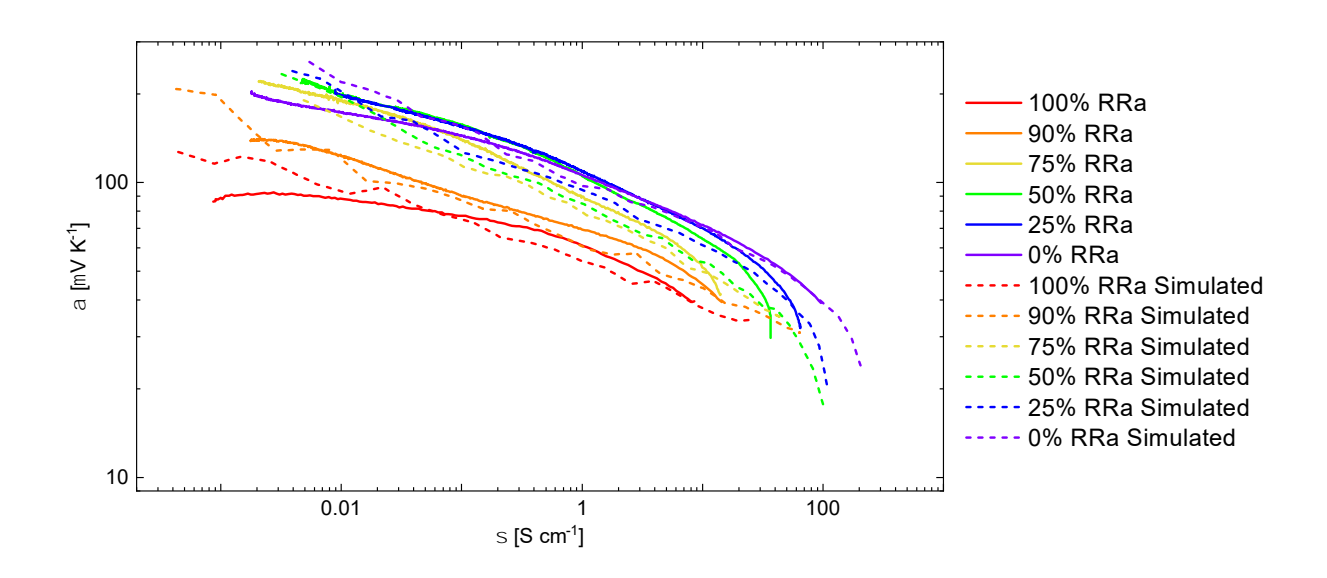


Figure 5: Experimental data and simulations estimate polymer-dopant distances. Experimental data of Seebeck coefficient (α) and electrical conductivity (σ) fits to simulated data. Simulated data of pure components were simulated using a polymer-dopant distance of 0.8 nm for regioregular P3HT and 0.3 nm for regiorandom P3HT. Thermoelectric properties of P3HT blends were simulated by combining the DOS of each component.

We then calculated α and σ at each carrier concentration using our simulation of phonon-assisted hopping in the generalized Gaussian disorder model (see Methods Section) and used that data to plot the α - σ curve in Figure 5. To qualitatively understand the impact of the distance

between the polaron and counterion (R_s) on the α - σ curves, we varied the R_s from 0.3 to 1 nm and observed a consistent shift to the upper-right on the plot, indicating that larger separation leads to weaker Coulomb interactions, shallower traps, and lower energetic disorder (see Figure S6), which is favorable to transport as carriers can hop more efficiently between states that are energetically closer. 11 When then fitted our model to the experimentally obtained α - σ curves for regionardom P3HT and regioregular P3HT, using the same procedure to obtain the DOS as for spectra and dedoping. For regiorandom P3HT, there is a single DOS because the material is structurally homogenous. 52 Regioregular P3HT was shown to have both crystalline and amorphous regions so we used a combination of one DOS for the crystalline and another for the amorphous domain, which were linearly added in a 1:1 ratio to obtain the total DOS. This ratio is based on experimental determination of crystallinity of commercial regionegular P3HT similar to ones used in this study using X-ray Diffraction and solid-state NMR.²⁹ Each DOS is then modified with Coulomb interactions from its corresponding doping concentration according to the model detailed in Methods. For regiorandom P3HT, our fits to the experimental α - σ data provide an R_s of 0.3 nm, while fits to regioregular P3HT provide an R_s of 0.8 nm, obtaining excellent agreement with both across the entire measured doping range. The R_s obtained this way is consistent with previous literature by Schwartz, et. al. that estimated a distance of 0.6-0.8 nm for regioregular P3HT with a different dopant. 46 It is likely that that a larger R_s is associated the stabilization of the radical cation through cation- π interaction or delocalization of the charge in the π stacks. This is consistent with our WAXS data that shows a decrease in the π - π stacking distance in regionegular P3HT and this decrease in the distance has been attributed to the delocalization of the charge in the π stacks.⁵³ To fit the α - σ data for the blends, we used a combination of the separate doped DOS of regionegular and regiorandom P3HT with the appropriate ratio corresponding to each blend.

Our two-DOS model accurately captures the trends in the α - σ curves with blending across the full range of doping, including changes in the slope and relative positions of these curves, without any further fitting. Our two-DOS model with the dopant-induced disorder also captures trends associated with the kinetics of dedoping, discussed previously, as the doping concentration in each region in the blend is computed from its corresponding dedoping rate. The picture that emerges is that each structural feature in the morphology of the conjugated polymer film contributes to transport through the DOS. The width of each initial DOS is determined by the molecular interactions and structural disorder in that structural feature. The extent of the dopant-induced disorder on each DOS is determined by the separation distance between the counterion and the polymer upon doping and the extent of doping. The closer the counterion, the larger the dopant-induced disorder. The slope of the α - σ curve is not a constant as predicted by the empirical power law, $\alpha \sim \sigma^{1/4}$, but changes according to the changes in the shape of the DOS due to dopant-induced disorder at that doping level. If the dopant-induced disorder causes a heavy exponential tail, then transport is suppressed and the slope of the α - σ curve is shallower.

Conclusions: In this work, we show that the polymer-dopant separation distance, R_s , is a reliable parameter that impacts dopant-induced disorder, which is evidenced in the shape and position of Seebeck-conductivity curves measured over a broad range of doping concentrations. In the regionandom P3HT, the smaller R_s contributes to a larger dopant-induced disorder, lowering both conductivity and Seebeck. In the regionegular P3HT, a larger R_s leads to lower dopant-induced disorder. The charge transport is dictated by both these DOS distributions and the location of the Fermi level upon doping. A two-DOS model with associated dopant-induced disorder in each region describes the observed trends in the α - σ curves for regionegular P3HT, regionandom P3HT and their blends. The model also captures the observed trends associated with the kinetics

of dedoping and the trends in polaron peak positions. Thus, to observe any trends in counterion size or paracrystallinity on impact charge transport, it has to sufficiently alter R_s . Our studies also show that the amorphous domain suffers a larger dopant-induced disorder but still contributes to charge transport. Thus it is important to take into account the dopant-induced disorder in the amorphous domains as we design polymers and dopants for improved charge transport.

ASSOCIATED CONTENT

Data Availability Statement

The data underlying this study are openly available in Scholarworks@UMassAmherst at DOI [Will be provided after acceptance]

Supporting Information.

The following file is available free of charge at: [Insert Link; upon acceptance]
Simulated DOS; associated error of simulated Seebeck-conductivity curves; X-ray scattering pattern peak deconvolution fits and log-lin plots; scattering peaks and their calculated g parameters; rate parameters for kinetic analysis; and simulated diffusion rates for polymer-dopant distances and energy level offset (PDF)

AUTHOR INFORMATION

Corresponding Authors

Dhandapani Venkataraman—Department of Chemistry and Materials Science and Engineering Interdisciplinary Graduate Program, University of Massachusetts Amherst, 690 N. Pleasant Street, Amherst, MA 01003. Email: dv@umass.edu

Zlatan Akšamija—Department of Materials Science and Engineering, University of Utah, 122 S. Central Campus Drive, Salt Lake City, Utah 84112-0056

Author Contributions

D.V and Z.A designed the overall study. D.V, and MLD designed the experiments with input from M.D and Z.A. Z.A and M.D performed the computations and simulations. M.L.D performed the dedoping experiments, measured α vs σ curves, characterized the morphology using X-ray scattering. M.D. fitted the experimental data charge transport models and extracted the density of states, computed the diffusion rates and absorption coefficients. S.H. and S.S. performed the kinetic analysis. M.L.D and S.H also characterized polymer films using UV-vis-NIR. The manuscript was written through contributions of all authors. All authors have given approval to the final version of the manuscript. \ddagger M.L.D and M.D contributed equally to this manuscript.

Funding Sources

National Science Foundation DMR 2101127

ACKNOWLEDGMENT

We thank the National Science Foundation DMR (Grant no. DMR 2101127) for financial support. We also thank Prof. Michael Barnes for insightful discussions on the analysis of the kinetics of dedoping.

ABBREVIATIONS

P3HT, poly(3-hexylthiophene); density of states, DOS.

REFERENCES

- (1) Liu, J.; Shi, Y. Q.; Dong, J. J.; Nugraha, M. I.; Qiu, X. K.; Su, M. Y.; Chiechi, R. C.; Baran, D.; Portale, G.; Guo, X. G.; et al. Overcoming Coulomb Interaction Improves Free-Charge Generation and Thermoelectric Properties for n-Doped Conjugated Polymers. *ACS Energy Lett.* **2019**, *4*, 1556-1564.
- (2) Zuo, G. Z.; Abdalla, H.; Kemerink, M. Impact of Doping on the Density of States and the Mobility in Organic Semiconductors. *Phys. Rev. B* **2016**, *93*, 235203.
- (3) Scholes, D. T.; Hawks, S. A.; Yee, P. Y.; Wu, H.; Lindemuth, J. R.; Tolbert, S. H.; Schwartz, B. J. Overcoming Film Quality Issues for Conjugated Polymers Doped with F₄-TCNQ by Solution Sequential Processing: Hall Effect, Structural, and Optical Measurements. *J. Phys. Chem. Lett.* **2015**, *6*, 4786-4793.
- (4) Pingel, P.; Neher, D. Comprehensive Picture of p-Type Doping of P3HT with the Molecular Acceptor F₄-TCNQ. *Phys. Rev. B* **2013**, *87*, 115209.
- (5) Arkhipov, V. I.; Emelianova, E. V.; Heremans, P.; Bässler, H. Analytic Model of Carrier Mobility in Doped Disordered Organic Semiconductors. *Phys. Rev. B* **2005**, *72*, 235202.
- (6) Arkhipov, V. I.; Heremans, P.; Emelianova, E. V.; Bässler, H. Effect of Doping on the Density-of-States Distribution and Carrier Hopping in Disordered Organic Semiconductors. *Phys. Rev. B* **2005**, *71*, 045214.
- (7) Salzmann, I.; Heimel, G.; Oehzelt, M.; Winkler, S.; Koch, N. Molecular Electrical Doping of Organic Semiconductors: Fundamental Mechanisms and Emerging Dopant Design Rules. *Accounts Chem. Res.* **2016**, *49*, 370-378.

- (8) Liang, Z. M.; Zhang, Y. D.; Souri, M.; Luo, X. Y.; Boehm, A. M.; Li, R. P.; Zhang, Y.; Wang, T. R.; Kim, D. Y.; Mei, J. G.; et al. Influence of Dopant Size and Electron Affinity on the Electrical Conductivity and Thermoelectric Properties of a Series of Conjugated Polymers. *J. Mater. Chem. A* **2018**, *6*, 16495-16505.
- (9) Shi, W.; Yildirim, E.; Wu, G.; Wong, Z. M.; Deng, T. Q.; Wang, J. S.; Xu, J. W.; Yang, S. W. The Role of Electrostatic Interaction between Free Charge Carriers and Counterions in Thermoelectric Power Factor of Conducting Polymers: From Crystalline to Polycrystalline Domains. *Adv. Theory Simul.* **2020**, *3*, 2000015.
- (10) Boyle, C. J.; Upadhyaya, M.; Wang, P. J.; Renna, L. A.; Lu-Díaz, M.; Jeong, S. P.; Hight-Huf, N.; Korugic-Karasz, L.; Barnes, M. D.; Aksamija, Z.; et al. Tuning Charge Transport Dynamics Via Clustering of Doping in Organic Semiconductor Thin Films. *Nat. Commun.* **2019**, *10*, 2827.
- (11) Upadhyaya, M.; Boyle, C. J.; Venkataraman, D.; Aksamija, Z. Effects of Disorder on Thermoelectric Properties of Semiconducting Polymers. *Sci Rep* **2019**, *9*, 5820.
- (12) Aubry, T. J.; Winchell, K. J.; Salamat, C. Z.; Basile, V. M.; Lindemuth, J. R.; Stauber, J. M.; Axtell, J. C.; Kubena, R. M.; Phan, M. D.; Bird, M. J.; et al. Tunable Dopants with Intrinsic Counterion Separation Reveal the Effects of Electron Affinity on Dopant Intercalation and Free Carrier Production in Sequentially Doped Conjugated Polymer Films. *Adv. Funct. Mater.* **2020**, *30*, 2001800.
- (13) Ju, D.; Kim, J.; Yook, H.; Han, J. W.; Cho, K. Engineering Counter-Ion-Induced Disorder of a Highly Doped Conjugated Polymer for High Thermoelectric Performance. *Nano Energy* **2021**, *90*, 106604.

- (14) Upadhyaya, M.; Lu-Díaz, M.; Samanta, S.; Abdullah, M.; Dusoe, K.; Kittilstved, K. R.; Venkataraman, D.; Aksamija, Z. Raising Dielectric Permittivity Mitigates Dopant-Induced Disorder in Conjugated Polymers. *Adv. Sci.* **2021**, *8*, 2101087.
- (15) Thomas, E. M.; Popere, B. C.; Fang, H. Y.; Chabinyc, M. L.; Segalman, R. A. Role of Disorder Induced by Doping on the Thermoelectric Properties of Semiconducting Polymers. *Chem. Mat.* **2018**, *30*, 2965-2972.
- (16) Thomas, E. M.; Peterson, K. A.; Balzer, A. H.; Rawlings, D.; Stingelin, N.; Segalman, R. A.; Chabinyc, M. L. Effects of Counter-Ion Size on Delocalization of Carriers and Stability of Doped Semiconducting Polymers. *Adv. Electron. Mater.* **2020**, *6*, 2000595.
- (17) Baustert, K. N.; Abtahi, A.; Ayyash, A. N.; Graham, K. R. Impact of the Anion on Electrochemically Doped Regioregular and Regiorandom Poly(3-Hexylthiophene). *J. Polym. Sci.* **2022**, *60*, 602-609.
- (18) Jacobs, I. E.; D'Avino, G.; Lemaur, V.; Lin, Y.; Huang, Y. X.; Chen, C.; Harrelson, T. F.; Wood, W.; Spalek, L. J.; Mustafa, T.; et al. Structural and Dynamic Disorder, Not Ionic Trapping, Controls Charge Transport in Highly Doped Conducting Polymers. *J. Am. Chem. Soc.* **2022**, *144*, 3005-3019.
- (19) Chen, C.; Jacobs, I. E.; Kang, K. H.; Lin, Y.; Jellett, C.; Kang, B. S.; Lee, S. B.; Huang, Y. X.; Qarai, M. B.; Ghosh, R.; et al. Observation of Weak Counterion Size Dependence of Thermoelectric Transport in Ion Exchange Doped Conducting Polymers across a Wide Range of Conductivities. *Adv. Energy Mater.* **2023**, *13*, 2202797.

- (20) Murrey, T. L.; Aubry, T. J.; Ruiz, O. L.; Thurman, K. A.; Eckstein, K. H.; Doud, E. A.; Stauber, J. M.; Spokoyny, A. M.; Schwartz, B. J.; Hertel, T.; et al. Tuning Counterion Chemistry to Reduce Carrier Localization in Doped Semiconducting Carbon Nanotube Networks. *Cell Rep. Phys. Sci.* **2023**, *4*, 101407.
- (21) Lim, E.; Glaudell, A. M.; Miller, R.; Chabinyc, M. L. The Role of Ordering on the Thermoelectric Properties of Blends of Regioregular and Regiorandom Poly(3-Hexylthiophene). *Adv. Electron. Mater.* **2019**, *5*, 1800915.
- (22) Venkateshvaran, D.; Nikolka, M.; Sadhanala, A.; Lemaur, V.; Zelazny, M.; Kepa, M.; Hurhangee, M.; Kronemeijer, A. J.; Pecunia, V.; Nasrallah, I.; et al. Approaching Disorder-Free Transport in High-Mobility Conjugated Polymers. *Nature* **2014**, *515*, 384-388.
- (23) Zhang, X. R.; Bronstein, H.; Kronemeijer, A. J.; Smith, J.; Kim, Y.; Kline, R. J.; Richter, L. J.; Anthopoulos, T. D.; Sirringhaus, H.; Song, K.; et al. Molecular Origin of High Field-Effect Mobility in an Indacenodithiophene-Benzothiadiazole Copolymer. *Nat. Commun.* **2013**, *4*, 2238.
- (24) Kim, G.; Pipe, K. P. Thermoelectric Model to Characterize Carrier Transport in Organic Semiconductors. *Phys. Rev. B* **2012**, *86*, 085208.
- (25) Kang, S. D.; Snyder, G. J. Charge-Transport Model for Conducting Polymers. *Nature Mater* **2017**, *16*, 252-257.
- (26) Baranovskii, S. D. Theoretical Description of Charge Transport in Disordered Organic Semiconductors. *Phys. Status Solidi B Basic Res.* **2014**, *251*, 487-525.

- (27) Rivnay, J.; Noriega, R.; Kline, R. J.; Salleo, A.; Toney, M. F. Quantitative Analysis of Lattice Disorder and Crystallite Size in Organic Semiconductor Thin Films. *Phys. Rev. B* **2011**, *84*, 045203.
- (28) Duhandžić, M.; Lu-Dìaz, M.; Samanta, S.; Venkataraman, D.; Akšamija, Z. Carrier Screening Controls Transport in Conjugated Polymers at High Doping Concentrations. *Phys. Rev. Lett.* **2023**, *131*, 248101.
- (29) Shen, X. B.; Hu, W. G.; Russell, T. P. Measuring the Degree of Crystallinity in Semicrystalline Regioregular Poly(3-Hexylthiophene). *Macromolecules* **2016**, *49*, 4501-4509.
- (30) Hood, S.; Zarrabi, N.; Meredith, P.; Kassal, I.; Armin, A. Measuring Energetic Disorder in Organic Semiconductors Using the Photogenerated Charge-Separation Efficiency. *J. Phys. Chem. Lett.* **2019**, *10*, 3863-3870.
- (31) Untilova, V.; Zeng, H. Y.; Durand, P.; Herrmann, L.; Leclerc, N.; Brinkmann, M. Intercalation and Ordering of F₆-TCNNQ and F₄-TCNQ Dopants in Regioregular Poly(3-Hexylthiophene) Crystals: Impact on Anisotropic Thermoelectric Properties of Oriented Thin Films. *Macromolecules* **2021**, *54*, 6073-6084.
- (32) Zhong, Y. H.; Untilova, V.; Muller, D.; Guchait, S.; Kiefer, C.; Herrmann, L.; Zimmermann, N.; Brosset, M.; Heiser, T.; Brinkmann, M. Preferential Location of Dopants in the Amorphous Phase of Oriented Regioregular Poly(3-Hexylthiophene-2,5-Diyl) Films Helps Reach Charge Conductivities of 3000 S Cm⁻¹. *Adv. Funct. Mater.* **2022**, *32*, 2202075.
- (33) Tsoi, W. C.; Spencer, S. J.; Yang, L.; Ballantyne, A. M.; Nicholson, P. G.; Turnbull, A.; Shard, A. G.; Murphy, C. E.; Bradley, D. D. C.; Nelson, J.; et al. Effect of Crystallization on the

Electronic Energy Levels and Thin Film Morphology of P3HT:PCBM Blends. *Macromolecules* **2011**, *44*, 2944-2952.

- (34) Tashiro, K.; Kobayashi, M.; Kawai, T.; Yoshino, K. Crystal Structural Change in Poly(3-Alkyl Thiophene)S Induced by Iodine Doping as Studied by an Organized Combination of X-Ray Diffraction, Infrared/Raman Spectroscopy and Computer Simulation Techniques. *Polymer* **1997**, *38*, 2867-2879.
- (35) Okamoto, T.; Kudoh, K.; Wakamiya, A.; Yamaguchi, S. General Synthesis of Extended Fused Oligothiophenes Consisting of an Even Number of Thiophene Rings. *Chem.-Eur. J.* **2007**, *13*, 548-556.
- (36) Lasher, G.; Stern, F. Spontaneous and Stimulated Recombination Radiation in Semiconductors. *Phys. Rev. A* **1964**, *133*, A553-A563.
- (37) Chew, A. R.; Ghosh, R.; Shang, Z. R.; Spano, F. C.; Salleo, A. Sequential Doping Reveals the Importance of Amorphous Chain Rigidity in Charge Transport of Semi-Crystalline Polymers. *J. Phys. Chem. Lett.* **2017**, *8*, 4974-4980.
- (38) Abdalla, H.; Zuo, G. Z.; Kemerink, M. Range and Energetics of Charge Hopping in Organic Semiconductors. *Phys. Rev. B* **2017**, *96*, 241202.
- (39) Hynynen, J.; Kiefer, D.; Müller, C. Influence of Crystallinity on the Thermoelectric Power Factor of P3HT Vapour-Doped with F₄TCNQ. *RSC Adv.* **2018**, *8*, 1593-1599.
- (40) Hynynen, J.; Järsvall, E.; Kroon, R.; Zhang, Y. D.; Barlow, S.; Marder, S. R.; Kemerink, M.; Lund, A.; Müller, C. Enhanced Thermoelectric Power Factor of Tensile Drawn Poly(3-Hexylthiophene). *ACS Macro Lett.* **2019**, *8*, 70-76.

- (41) Ma, T. Z.; Dong, B. X.; Grocke, G. L.; Strzalka, J.; Patel, S. N. Leveraging Sequential Doping of Semiconducting Polymers to Enable Functionally Graded Materials for Organic Thermoelectrics. *Macromolecules* **2020**, *53*, 2882-2892.
- (42) Scheunemann, D.; Vijayakumar, V.; Zeng, H. Y.; Durand, P.; Leclerc, N.; Brinkmann, M.; Kemerink, M. Rubbing and Drawing: Generic Ways to Improve the Thermoelectric Power Factor of Organic Semiconductors? *Adv. Electron. Mater.* **2020**, *6*, 2000218.
- (43) Liu, J.; Qiu, L.; Portale, G.; Torabi, S.; Stuart, M. C. A.; Qiu, X. K.; Koopmans, M.; Chiechi, R. C.; Hummelen, J. C.; Koster, L. J. A. Side-Chain Effects on N-Type Organic Thermoelectrics: A Case Study of Fullerene Derivatives. *Nano Energy* **2018**, *52*, 183-191.
- (44) Wang, S. H.; Sun, H. D.; Ail, U.; Vagin, M.; Persson, P.; Andreasen, J. W.; Thiel, W.; Berggren, M.; Crispin, X.; Fazzi, D.; et al. Thermoelectric Properties of Solution-Processed n-Doped Ladder-Type Conducting Polymers. *Adv. Mater.* **2016**, *28*, 10764-10771.
- (45) Zuo, G. Z.; Li, Z. J.; Wang, E. G.; Kemerink, M. High Seebeck Coefficient and Power Factor in n-Type Organic Thermoelectrics. *Adv. Electron. Mater.* **2018**, *4*, 1700501.
- (46) Yee, P. Y.; Scholes, D. T.; Schwartz, B. J.; Tolbert, S. H. Dopant-Induced Ordering of Amorphous Regions in Regionandom P3HT. *J. Phys. Chem. Lett.* **2019**, *10*, 4929-4934.
- (47) Lim, E.; Peterson, K. A.; Su, G. M.; Chabinyc, M. L. Thermoelectric Properties of Poly(3-Hexylthiophene) (P3HT) Doped with 2,3,5,6-Tetrafluoro-7,7,8,8-Tetracyanoquinodimethane (F4-TCNQ) by Vapor-Phase Infiltration. *Chem. Mat.* **2018**, *30*, 998-1010.

- (48) Peng, Z. X.; Ye, L.; Ade, H. Understanding, Quantifying, and Controlling the Molecular Ordering of Semiconducting Polymers: From Novices to Experts and Amorphous to Perfect Crystals. *Mater. Horizons* **2022**, *9*, 577-606.
- (49) Scholes, D. T.; Yee, P. Y.; Lindemuth, J. R.; Kang, H.; Onorato, J.; Ghosh, R.; Luscombe, C. K.; Spano, F. C.; Tolbert, S. H.; Schwartz, B. J. The Effects of Crystallinity on Charge Transport and the Structure of Sequentially Processed F₄TCNQ-Doped Conjugated Polymer Films. *Adv. Funct. Mater.* **2017**, *27*, 1702654.
- (50) Wu, E. C.; Salamat, C. Z.; Ruiz, O. L.; Qu, T.; Kim, A.; Tolbert, S. H.; Schwartz, B. J. Counterion Control and the Spectral Signatures of Polarons, Coupled Polarons, and Bipolarons in Doped P3HT Films. *Adv. Funct. Mater.* **2023**, *33*, 2213652.
- (51) Noriega, R.; Rivnay, J.; Vandewal, K.; Koch, F. P. V.; Stingelin, N.; Smith, P.; Toney, M. F.; Salleo, A. A General Relationship between Disorder, Aggregation and Charge Transport in Conjugated Polymers. *Nature Mater* **2013**, *12*, 1038-1044.
- (52) Shen, X. B.; Duzhko, V. V.; Russell, T. P. A Study on the Correlation between Structure and Hole Transport in Semi-Crystalline Regionegular P3HT. *Adv. Energy Mater.* **2013**, *3*, 263-270.
- (53) Liu, W.; Müller, L.; Ma, S.; Barlow, S.; Marder, S. R.; Kowalsky, W.; Köhn, A.; Lovrincic,
 R. Origin of the π–π Spacing Change Upon Doping of Semiconducting Polymers. *J. Phys. Chem.*C 2018, 122, 27983-27990.

TOC GRAPHIC

